

Capturing electronic correlations in electron-phonon interactions in molecular systems with the GW approximation

Antonios M. Alvertis^{1,2,*}, David B. Williams-Young³, Fabien Bruneval⁴, Jeffrey B. Neaton^{2,5,6,†}

¹KBR, Inc., NASA Ames Research Center, Moffett Field, California 94035, United States

²Materials Sciences Division, Lawrence Berkeley National Laboratory, Berkeley, California 94720, United States

³Applied Mathematics and Computational Research Division, Lawrence Berkeley National Laboratory, Berkeley, California 94720, United States

⁴Université Paris-Saclay, CEA, Service de Corrosion et de Comportement des Matériaux, SRMP, 91191 Gif-sur-Yvette, France

⁵Department of Physics, University of California Berkeley, Berkeley, United States

⁶Kavli Energy NanoScience Institute at Berkeley, Berkeley, United States

*e-mail: amalvertis@lbl.gov

†e-mail: jbneaton@lbl.gov

Abstract

Electron-phonon interactions are of great importance to a variety of physical phenomena, and their accurate description is an important goal for first-principles calculations. Isolated examples of materials and molecular systems have emerged where electron-phonon coupling is enhanced over density functional theory (DFT) when using the Green's-function-based *ab initio* GW method, which provides a more accurate description of electronic correlations. It is however unclear how general this enhancement is, and how employing high-end quantum chemistry methods, which further improve the description of electronic correlations, might further alter electron-phonon interactions over GW or DFT. Here, we address these questions by computing the renormalization of the highest occupied molecular orbital energies of Thiel's set of organic molecules by harmonic vibrations using DFT, GW and equation-of-motion coupled-cluster calculations. We find that GW can increase the magnitude of the electron-phonon coupling across this set of molecules by an average factor of 1.1 – 1.8 compared to DFT, while equation-of-motion coupled-cluster leads to an increase of 1.4 – 2. The electron-phonon coupling predicted with the *ab initio* GW method is generally in much closer agreement to coupled cluster values compared to DFT, establishing GW as an accurate way of computing electron-phonon phenomena in molecules and beyond at a much lower computational cost than higher-end quantum chemistry techniques.

1 Introduction

The interaction of electrons with atomic and lattice vibrations (phonons) in solids is of central importance in chemistry and physics, defining carrier transport properties [1, 2], superconducting critical temperatures [3, 4], the rate of non-radiative recombination [5, 6], the reaction pathway of ultrafast charge and energy transfer [7, 8], and more for materials and molecular systems. In organic molecules and molecular crystals, atomic and lattice vibrations can cause substantial renormalization of ground and excited state properties [9, 10, 11, 12]. Therefore, accurate and predictive theories for the interaction of electrons with vibrations are important in order to guide the experimental search for systems with a wide range of functionality, as well as to promote the fundamental understanding of a variety of physical processes.

For decades, density functional theory (DFT) has arguably been the most widely used framework for computing the properties of molecules and materials from first principles, and it has been extensively used to calculate electronic and vibrational degrees of freedom, as well as their interplay [13, 14, 15, 16, 17]. The choice of the DFT exchange-correlation functional has been known in several systems to affect the predicted magnitude of these effects, with examples demonstrating that inclusion of exact exchange to the DFT functional tends to increase electron-phonon coupling [18] compared to cases where the local density approximation (LDA) [19] and generalized gradient approximations (GGA) [20] are used. Moreover, *ab initio* many-body perturbation theory within the *GW* approximation [21, 22], which is known to yield highly accurate properties for the electronic levels of molecular systems and solids [23, 24, 25, 26, 27, 28, 29, 30, 31, 32, 33, 34, 35, 36, 37, 38, 39, 40, 41, 42, 43, 44, 45], has also been used to compute electron-phonon coupling, showing significantly increased magnitude of these interactions over DFT in some cases [46, 47, 48, 49, 50], but only small changes in others [49]. Further increases of electron-phonon coupling might also be expected with an even more accurate description of electronic correlations, *e.g.* methods such as coupled cluster (CC) [51]. Additionally, the challenge associated with rigorously converging electron-phonon calculations in solids has led to the suggestion that the discrepancies reported in the literature in the phonon-induced fundamental gap renormalization obtained at different levels of electronic structure theory could potentially be attributed to under-converged calculations [52]. Given these practical challenges and inconclusive reports, there remains no consensus on whether including exact exchange within DFT or employing higher-level *GW* calculations leads to a systematic increase of the computed electron-phonon interactions, or whether examples in the literature showing such an increase constitute isolated cases. To complicate matters further, Kohn-Sham wavefunctions computed within DFT are most commonly used as a starting point for *GW* calculations, and the choice of starting point can greatly affect the *GW* results [53, 54]. However, the dependence of the electron-phonon interactions computed with *GW* on the functional employed for the DFT starting point remains unknown.

Here we present a systematic study of electron-phonon coupling using Thiel’s set of organic molecules [55], a set of 28 small molecules. As a proxy for the magnitude of the coupling of molecular vibrations to electrons, we study the renormalization of the highest occupied molecular orbital (HOMO) energy of each molecule due to the zero-point motion of the atomic nuclei, which we obtain within the harmonic approximation using a

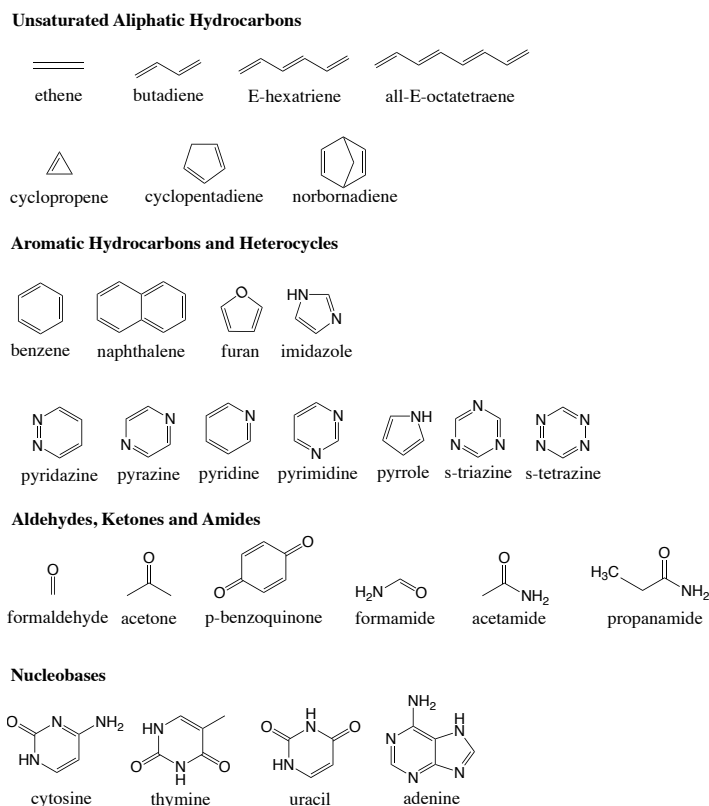


Figure 1 Thiel's set of organic molecules.

well-established finite-displacements approach [56, 9]. We compute the zero-point renormalization (ZPR) of the HOMO energies with DFT using several different functionals with varying degrees of exact exchange, and we also perform *GW* calculations with various DFT starting points. We compare our DFT and *GW* ZPR calculations to the values obtained with accurate coupled-cluster (CC) methods. Our results establish that the correction to DFT electronic correlations obtained within the *GW* and CC formalisms tends to systematically increase the magnitude of electron-phonon coupling, particularly when employing DFT functionals with semilocal or small amounts of exact exchange. That *GW* and CC methods generally predict stronger electron-phonon interactions compared to DFT can have implications for accurate prediction of properties such as superconductivity [47, 50] and finite-temperature excited state properties [57] in other systems. The results with *GW* are in overall good agreement with CC, yet obtained at much lower computational cost (N^4 compared to N^6 for coupled cluster), suggesting that the *GW* method provides a powerful and computationally efficient way of accurately modeling electron-phonon interactions in molecular systems.

2 Theoretical background and computational methods

In this paper we study the so-called Thiel's set of organic molecules shown in Fig. 1, which consists of 28 diverse gas-phase molecular structures [55]. In order to understand the impact of the level of the electronic structure theory on the magnitude of the electron-phonon interactions, we focus on the vibrationally-induced ZPR of the

HOMO energy of the Thiel’s set molecules. Section 2.1 provides an overview of the theoretical framework we employ here. Then Section 2.2 goes into some detail on the electronic structure methods used in this work in order to compute the HOMO energies of the Thiel’s set molecules, and Section 2.3 summarizes the results of our vibrational and electronic structure calculations to compute the HOMO ZPR at the various levels of theory.

2.1 Vibrational averages of observables

In what follows, we review the formalism for computing vibrational averages for quantum-mechanical operators, and some of the approximations relevant to this work. Let us consider an operator \mathcal{O} corresponding to an observable of interest, in the presence of atomic motion at temperature T . Within the Born-Oppenheimer approximation, the finite-temperature expectation value of \mathcal{O} may be written as

$$\langle \mathcal{O}(T) \rangle_{\mathcal{H}} = \frac{1}{Z} \int dX \mathcal{O}(X) e^{-\beta \mathcal{H}}, \quad (1)$$

where the canonical partition function $Z = \int dX e^{-\beta \mathcal{H}}$ involves the configuration space integral $\int dX$ [58].

The Hamiltonian \mathcal{H} of the system includes electronic and nuclear degrees of freedom in general, and may be approximated at different levels. One approach that is generally valid for small organic molecules is to assume nuclear motion to be harmonic, reducing the vibrational contribution to the Hamiltonian to the following form,

$$\mathcal{H}^{\text{har}} \equiv \frac{1}{2} \sum_n (\nabla_{u_n}^2 + \omega_n^2 u_n^2), \quad (2)$$

in atomic units. Here, ω_n is the frequency of the n_{th} vibrational mode, and u_n the respective eigendisplacement, which are computed using a finite-displacements approach [59, 60] in conjunction with DFT total energy and forces calculations. The ground state vibrational properties of organic molecules are known to be fairly insensitive to the amount of exact exchange in the employed DFT functional [18], and we therefore compute the vibrational modes and frequencies of all structures considered here with the global hybrid B3LYP [61], as implemented in the NWChem software [62].

In the harmonic approximation, the integral of eq. 1 becomes [56]

$$\langle \mathcal{O}(T) \rangle_{\mathcal{H}} = \int d\mathbf{u} |\Phi(\mathbf{u}; T)|^2 \mathcal{O}(\mathbf{u}), \quad (3)$$

where \mathbf{u} a vector of atomic displacements associated with a given vibrational mode in the system and

$$|\Phi(\mathbf{u}; T)|^2 = \prod_n (2\pi\sigma_n^2(T))^{-1/2} \exp\left\{-\frac{u_n^2}{2\sigma_n^2(T)}\right\} \quad (4)$$

is the harmonic density at temperature T , which in turn is a product of Gaussian functions of width,

$$\sigma_n^2(T) = \frac{1}{2\omega_n} \cdot \coth\left(\frac{\omega_n}{2k_B T}\right). \quad (5)$$

The expectation value of eq. 3 may be computed by a Monte Carlo sampling, drawing N random samples \mathbf{u}_i from the harmonic density distribution function of eq. 4, at which we compute the observable of interest $\mathcal{O}(\mathbf{u}_i)$, allowing us to finally obtain

$$\langle \mathcal{O}(T) \rangle_{\text{MC}} = \lim_{N \rightarrow \infty} \frac{1}{N} \sum_{i=1}^N \mathcal{O}(\mathbf{u}_i). \quad (6)$$

This Monte Carlo (MC) sampling of the expectation value of observables has strong parallels to the nuclear ensemble method [63].

Apart from the harmonic and adiabatic approximations, no further assumptions have been made in deriving eq. 6. The Monte Carlo sampling method has the advantage of including the effect of vibrations to all orders on the observable of interest in a non-perturbative fashion [64]. We will focus here on the effect of vibrations on electronic observables (see Section 2.2) and refer to the interactions between electronic and vibrational degrees of freedom as electron-phonon interactions, and use the term “phonon” interchangeably with “molecular vibrations” and “normal modes”.

The Monte Carlo sampling method does not allow one to identify the contribution of individual vibrational modes to the thermal average, as we always consider collective displacements. In order to isolate the effect of individual vibrations one can expand the observable of interest in a specific vibrational coordinate as

$$\mathcal{O}(\mathbf{u}) = \mathcal{O}(\mathbf{0}) + \sum_n \frac{\partial \mathcal{O}(\mathbf{0})}{\partial u_n} u_n + \frac{1}{2} \sum_n \sum_{n'} \frac{\partial^2 \mathcal{O}(\mathbf{0})}{\partial u_n \partial u_{n'}} u_n u_{n'} + \dots, \quad (7)$$

where $\mathbf{u} = \mathbf{0}$ represents the equilibrium geometry of the molecule. In the above expansion of $\mathcal{O}(\mathbf{u})$ the third-order term vanishes, hence by truncating eq. 3 to fourth order one arrives at the so-called quadratic (Q) expectation value:

$$\langle \mathcal{O}(T) \rangle_{\text{Q}} = \mathcal{O}(\mathbf{0}) + \sum_n \frac{1}{2\omega_n} \cdot \frac{\partial^2 \mathcal{O}}{\partial u_n^2} \left[\frac{1}{2} + n_B(\omega_n, T) \right], \quad (8)$$

where $n_B(\omega_n, T)$ is the Bose-Einstein distribution function for the occupation of mode n at temperature T . At a practical level, the expectation value of eq. 8 may be obtained by approximating the second derivative appearing for every vibrational mode in this equation by the finite-difference formula

$$\frac{\partial^2 \mathcal{O}}{\partial u_n^2} \approx \frac{\mathcal{O}(\delta u_n) + \mathcal{O}(-\delta u_n) - 2\mathcal{O}(\mathbf{0})}{\delta u_n^2}. \quad (9)$$

The quadratic expectation value of eq. 8 is less accurate than the Monte Carlo expectation value of eq. 6, and also has the disadvantage that the finite difference formula employed to approximate the second derivative introduces some dependence on the choice of δu_n for every mode. While we will not use this level of approximation to extract quantitative values of observables in the presence of molecular vibrations, it offers the advantage of separating the contribution of each normal mode, and we will employ it below to gain further physical insights into the ZPR we compute with eq. 6.

2.2 Electronic structure calculation of molecular ionization potentials

Here we are interested in understanding the effect of vibrations on the HOMO energies, ϵ_{HOMO} , of the Thiel’s set molecules, therefore we take $\mathcal{O} = \epsilon_{\text{HOMO}}$, using the notation of Section 2.1. We compute all HOMO energies with DFT using a range of exchange-correlation functionals. Specifically, we employ the GGA as formulated by Perdew and Burke and Ernzerhof (PBE) [20]; and we employ global hybrid variants of PBE, namely PBEh(α), that contain a finite amount of exact exchange that is governed by the parameter α ranging from 0 to 1, namely

$$E_{XC} = \alpha E_X^{EX} + (1 - \alpha) E_X^{PBE} + E_C^{PBE}, \quad (10)$$

where E_{XC} the PBEh exchange-correlation functional, E_X^{EX} the exact exchange energy, and E_X^{PBE} and E_C^{PBE} are the PBE exchange and correlation energies respectively. We consider two cases, $\alpha = 0.25$ and $\alpha = 0.5$, in order to gain insights into the impact of the amount of exact exchange on the HOMO energies and their ZPR in this set of molecules. The case with $\alpha = 0.25$ is also referred to as the PBE0 functional, and we will refer to the case with $\alpha = 0.5$ simply as the PBEh functional. Moreover, we employ the BHLYP functional [65], which also contains 50% exact exchange. Functionals with about 50 % are known to provide an excellent starting point for subsequent *GW* calculations [31, 45] for molecular systems.

Beyond DFT, we also perform *GW* calculations using the so-called one-shot G_oW_o approach. Here the one-particle Green’s functions G and screened Coulomb interaction W are constructed from the eigenvalues and eigenvectors of a preceding DFT calculation (W is obtained within the random phase approximation [66]), and used to construct the self-energy $\Sigma = iGW$, which in turn is used to generate quasiparticle energies via correction $\Sigma - V_{XC}$ to generalized Kohn-Sham eigenvalues. Within this one-shot approach, we do not iteratively update Σ based on the computed *GW* eigenvalues and eigenvectors, as the one-shot G_oW_o approach has been shown to produce highly accurate results for a wide range of molecular systems [45]. While larger basis sets are often required to achieve convergence of the orbital energies obtained within *ab initio* many-body perturbation theory [67], the ZPR is computed as a difference between orbital energies (see eq. 12 below), which converges faster. In the supplementary information Fig. 1 and Fig. 2 we plot the convergence of the HOMO energy and HOMO ZPR respectively, for the example case of pyrimidine, with respect to the basis set size. We thus verify that the aug-cc-pVTZ basis produces converged results for the HOMO energy ZPR, which are at most 1 meV different from the values obtained using aug-cc-pV5Z.

In order to assess the accuracy of the computed DFT and *GW* HOMO energy ZPR in this work, we compare their values to the ZPR of the ionization potential (IP) as computed by the equation-of-motion ionization potential coupled cluster method with single and double excitations (EOM-IP-CCSD) [51]. For each of the molecules in Thiel’s set, we compute the lowest IP within EOM-IP-CCSD, corresponding to the negative of the HOMO energy according to the ionization potential theorem. We perform all EOM calculations within the Massively Parallel Quantum Chemistry (MPQC) code [68, 69], employing the aug-cc-pVTZ basis set as in the case of our DFT and *GW* calculations.

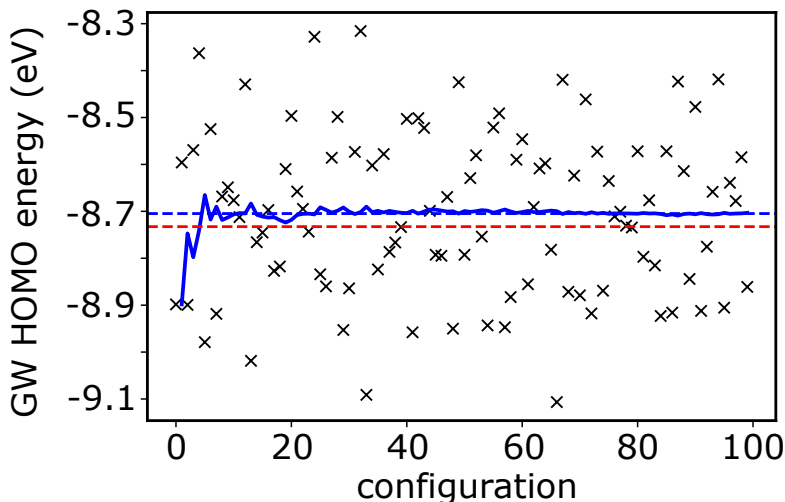


Figure 2 HOMO energies (black crosses) of furan (C_4H_4O) at different 0 K configurations, computed with one-shot $GW@PBE0$. The red dashed line indicates the HOMO energy in the absence of molecular vibrations, the blue dashed line is its converged 0 K value when vibrations are accounted for, and the blue solid line represents the cumulative average of the vibrational average of the HOMO energy.

2.3 Extracting the HOMO energy ZPR

We now combine the vibrational and electronic structure calculations of Sections 2.1 and 2.2 to compute the HOMO energy ZPR with different levels of electronic structure theory. For each molecule within the Thiel’s set, we generate $N = 100$ displaced configurations \mathbf{u}_i , and following eq. 6, we obtain the HOMO energy at 0 K as

$$\epsilon_{\text{HOMO}}(0\text{K})_{\text{MC}} = \frac{1}{100} \sum_{i=1}^{100} \epsilon_{\text{HOMO}}(\mathbf{u}_i). \quad (11)$$

The values of $\epsilon_{\text{HOMO}}(\mathbf{u}_i)$ are computed within the different levels of electronic structure theory outlined in Section 2.2. We find that $N = 100$ is generally sufficient to converge these vibrational averages, with values in the proximity of $N = 50$ already being converged within 1 meV in most cases. In Fig. 2 we show an example of the convergence of the HOMO energy of furan at 0 K with $GW@PBE0$ (one-shot GW with PBE0 eigenenergies and eigenstates as starting point).

The ZPR for the HOMO energy of each molecule is then obtained as

$$\text{ZPR} = \epsilon_{\text{HOMO}}(0\text{K}) - \epsilon_{\text{HOMO}}(\mathbf{u} = \mathbf{0}). \quad (12)$$

We note that for certain limited cases of molecules, and depending on the employed DFT functional, there can be accidental near-degeneracies between HOMO and HOMO-1, and the displacements \mathbf{u}_i can sometimes induce a change in the ordering of these orbitals. In order to reliably apply eq. 12, one needs to correctly identify the orbital that corresponds to the original HOMO, which we achieve by monitoring the expectation value of the kinetic energy operator of the near-degenerate orbitals. This case of accidental near-degeneracies is different to the symmetry-imposed degeneracy of molecules such as benzene, where the HOMO and HOMO-1 are degenerate. In these latter degenerate cases, the ZPR of the HOMO and HOMO-1 is taken to be the average

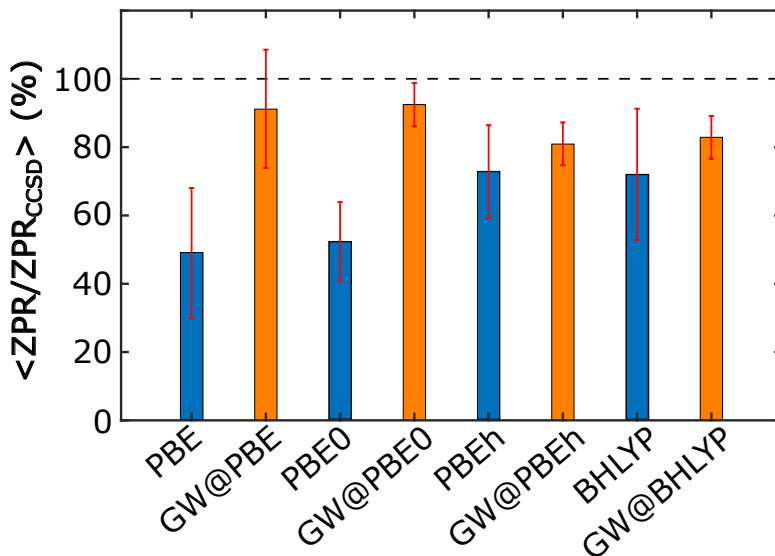


Figure 3 Average ratio (%) of the HOMO energy ZPR obtained at the different levels of theory compared with that obtained with EOM-IP-CCSD, across the entire Thiel’s set with the exception of butadiene, cyclopentadiene and naphthalene (see main text). Blue bars indicate the average ratio of the DFT HOMO energy ZPR values to EOM-IP-CCSD, while orange bars correspond to the respective *GW* values. The red bars are the standard error to the average values. Values near 100% correspond to good agreement with EOM-IP-CCSD.

Level of theory	MSE	MAE
PBE	−26.9	32.8
<i>GW</i> @PBE	2.9	11.1
PBE0	−18.7	18.8
<i>GW</i> @PBE0	−0.1	6.9
PBEh	−5.5	14.0
<i>GW</i> @PBEh	−5.9	8.9
BHLYP	−7.8	20.3
<i>GW</i> @BHLYP	−5.0	8.6

Table 1 Mean signed error (MSE) and mean absolute error (MAE) for the ZPR values at the different DFT and *GW* levels of electronic structure theory with respect to the ZPR values of our EOM-IP-CCSD reference. All values are in meV.

of the two, which is a gauge-invariant quantity.

3 Results and discussion

In Fig. 3 we show the average (across the Thiel’s set) of the ratio of the HOMO energy ZPR at the various DFT and *GW* levels of theory to the ZPR obtained within EOM-IP-CCSD (ZPR_{CCSD}). Table 1 gives the mean absolute error (MAE) and mean signed error (MSE) of the ZPR at the different levels of theory with respect to our EOM-IP-CCSD reference values. All ZPR values for the HOMO energies of individual molecules are given in the supplementary material. We have excluded butadiene, cyclopentadiene and naphthalene from the averages of Fig. 3, due to the fact that their EOM-IP-CCSD ZPR value is smaller than 2 meV, causing unphysically large oscillations in the values of the ratio presented in Fig. 3.

We first comment on the average ratio of the ZPR obtained using DFT with the various functionals to ZPR_{CCSD} , indicated with blue bars in Fig. 3. On average, as the content of exact exchange included in the

functional is increased, the magnitude of the ZPR increases, approaching the EOM-IP-CCSD values. This is consistent with reports in the literature for the fullerene C_{60} [18], where employing a hybrid functional increases the magnitude of electron-phonon interactions. Our result here shows that such a trend seems to hold generally across diverse organic molecules. This trend of increased ZPR with greater contents of exact exchange is consistent with the well-known increase in the electronic localization in Hartree-Fock compared to semi-local DFT [70]. The inclusion of exact exchange causes increased localization between bonded atoms, consequently resulting in greater variation of this density upon displacement of atoms, for example through carbon-carbon stretching motions. Such high-frequency motions dominate in small organic molecules such as the ones studied here, and are indeed known to have a larger effect on electronic states with a more localized electronic density [9, 10]. However, we note the inclusion of exact exchange is not sufficient to yield good agreement with the EOM-IP-CCSD ZPR values on average.

We now comment on the effect of performing GW calculations on top of the different DFT starting points. The average GW HOMO energy ZPR ratios to ZPR_{CCSD} in Fig. 3 (orange bars) show an increase compared to their DFT counterparts in each case. This effect is particularly prominent in the cases where functionals with a low exchange content (PBE and PBE0) are employed, with the average ZPR ratio increasing by a factor of 1.7–1.8 in these two cases compared to DFT. This strong systematic increase of the electron-phonon interactions predicted by GW compared to that computed from DFT functionals with low exchange content is consistent with multiple reports in the literature for diverse systems [46, 47, 48, 49, 50]. In fact, Refs. [46, 47, 48, 49, 50] all employ DFT starting points without any exact exchange. We also see from Fig. 3 that the increase of the HOMO energy ZPR from DFT to GW persists even in cases with 50% exact exchange (PBEh and BHLYP), although it is a much weaker effect compared to using functionals with a small content of exchange. The increase of electron-phonon interactions upon inclusion of exact exchange can in part reproduce the increase computed with GW . We note that the GW HOMO energy ZPR values have significantly smaller standard errors relative to DFT (with the exception of $GW@PBE$), highlighting the overall better performance of GW , even over hybrid DFT calculations with substantial exact exchange included. The additional electronic correlations included in EOM-IP-CCSD also lead to a small increase over GW . Notably, GW calculations on top of DFT starting points with no/low contents of exact exchange (PBE and PBE0 in this case) perform best in terms of reproducing the EOM-IP-CCSD reference.

In order to gain a better understanding of the ZPR averages of Fig. 3 and the large increase of the ZPR when performing GW calculations using PBE and PBE0 DFT starting points, we plot in Fig. 4 the HOMO energy ZPR with PBE and $GW@PBE$ (panel **a**) and with PBE0 and $GW@PBE0$ (panel **b**), against the EOM-IP-CCSD ZPR for each of the Thiel’s set molecules. It is evident that GW HOMO energy ZPR values are in better agreement with EOM-IP-CCSD, and are generally larger in magnitude compared DFT. Additionally, the GW ZPR values are more closely distributed around the black dashed line along the diagonal, indicating full agreement with EOM-IP-CCSD values, especially in the $GW@PBE0$ case.

We also identify the effect of individual vibrational modes on the ZPR differences at the different levels of theory. In Fig. 5 we show results for furan, where by using the quadratic approximation of Section 2.1 to the

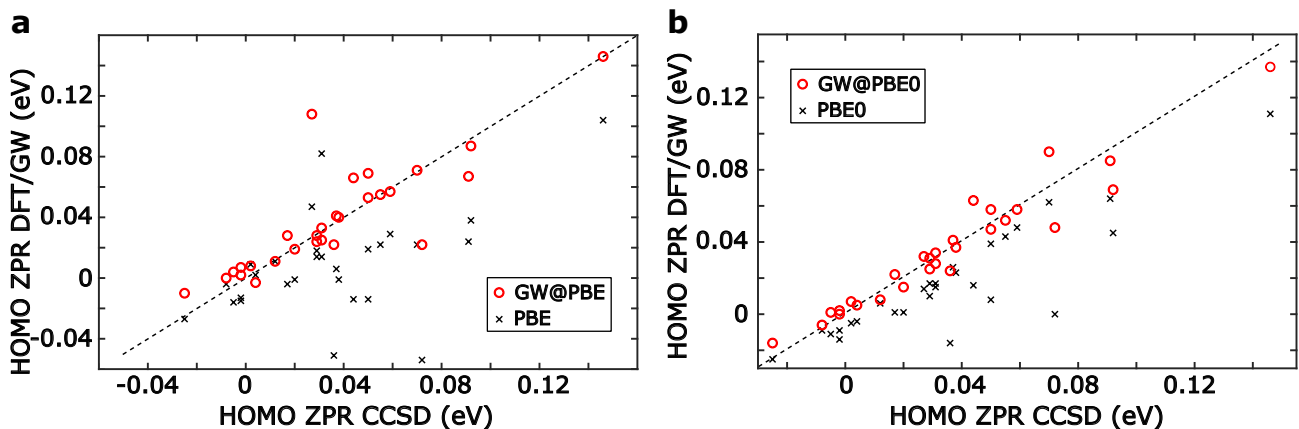


Figure 4 Comparison of the HOMO ZPR of the Thiel’s set molecules computed with PBE/*GW*@PBE (panel **a**) and PBE0/*GW*@PBE0 (panel **b**) to EOM-IP-CCSD values. Perfect agreement is indicated by the diagonal line (black dashes).

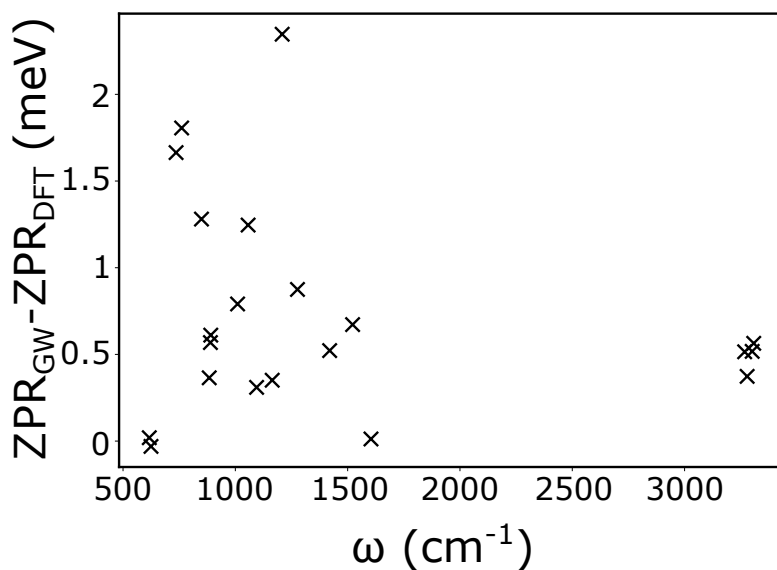


Figure 5 Vibrational mode-resolved difference in the ZPR computed with DFT PBE0 and *GW*@PBE0 for furan.

ZPR, we plot the difference between the PBE0 and *GW*@PBE0 HOMO energy ZPR values decomposed into the different normal mode contributions. Furan is representative of a more general phenomenon, where every individual mode tends to contribute increased ZPR at the *GW* level of theory compared to DFT. This is in agreement with the previous finding in the case of C_{60} [18], where employing a hybrid functional caused an increase of the electron-phonon coupling constants for the majority of the vibrational modes of the molecule.

Conclusions

We have presented a systematic study of the zero-point renormalization of the HOMO energy of the Thiel’s set of organic molecules computed at different levels of theory, in particular using DFT functionals with varying degree of exact exchange, *GW* calculations using these DFT calculations as starting points, and coupled-cluster calculations within the equation of motion formalism. We find that DFT HOMO energy ZPR values

are systematically underestimated compared to coupled-cluster values, with the inclusion of exact exchange somewhat improving agreement. HOMO energy ZPR values obtained within the *GW* formalism greatly increase the electron-phonon interactions predicted by the DFT starting points and result in much better agreement with coupled-cluster. The underestimation of the DFT ZPR is greatest when employing functionals with low fractions of exact exchange, in agreement with examples that have been reported in the literature over the past decade. Our study establishes such an increase in the magnitude of electron-phonon coupling to be a general feature of the *GW* method for molecules, and through comparison to coupled-cluster calculations emphasizes that indeed computing electron-phonon interactions within methods that incorporate electronic correlations beyond DFT is a necessary step towards achieving predictive accuracy for these phenomena. Importantly, the favorable scaling of *GW* calculations compared to coupled cluster demonstrates that *ab initio GW* methods can be more affordable and yet accurate for modeling electron-phonon interactions. Our results may have implications beyond molecular physics and for a wide range of systems in condensed matter, where electron-phonon interactions play an important role, including, but not limited to, molecular crystals and materials with potential for high-temperature superconductivity.

Acknowledgments

This work was undertaken as part of the Photosynthetic Light Harvesting program at LBNL and primarily supported by the U.S. Department of Energy, Basic Energy Sciences, Chemical Sciences, Geosciences, and Biosciences Division, under Contract No. DE-AC02-05CH11231. DWY was supported by the Center for Scalable Predictive methods for Excitations and Correlated phenomena (SPEC), which is funded by the U.S. Department of Energy (DoE), Office of Science, Office of Basic Energy Sciences, Division of Chemical Sciences, Geosciences and Biosciences as part of the Computational Chemical Sciences (CCS) program at Lawrence Berkeley National Laboratory under FWP 12553. This research used resources of the National Energy Research Scientific Computing Center (NERSC), a Department of Energy Office of Science User Facility using NERSC award BES-ERCAP0023385. Part of this work was performed using HPC resources from GENCI-TGCC (Grant 2023-gen6018).

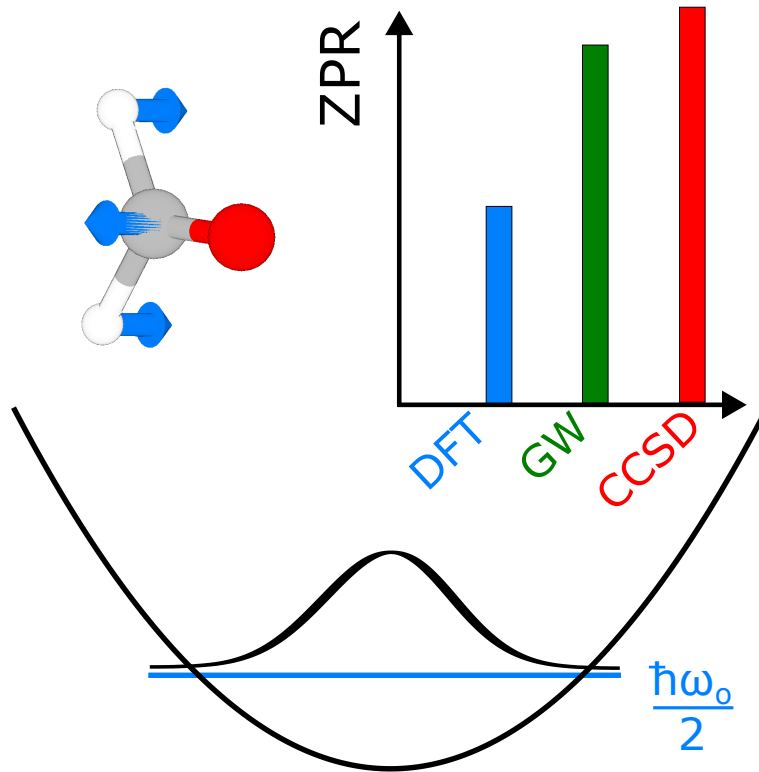


Figure 6 Table of contents figure.

References

- [1] Edward J. O'Reilly and Alexandra Olaya-Castro. Non-classicality of the molecular vibrations assisting exciton energy transfer at room temperature. *Nature Communications*, 5:1–10, 2014.
- [2] Katharina J. Franke and Jose Ignacio Pascual. Effects of electron-vibration coupling in transport through single molecules. *Journal of Physics Condensed Matter*, 24(39), 2012.
- [3] W.L. McMillan. Transition Temperature of Strong-Coupled Superconductors. *Physical Review*, 167(2):331, 1968.
- [4] P. B. Allen and R. C. Dynes. Transition temperature of strong-coupled superconductors reanalyzed. *Physical Review B*, 12(3):905–922, 1975.
- [5] Lin Shi and Lin Wang Wang. Ab initio calculations of deep-level carrier nonradiative recombination rates in bulk semiconductors. *Physical Review Letters*, 109(24):1–5, 2012.
- [6] Lin Shi, Ke Xu, and Lin Wang Wang. Comparative study of ab initio nonradiative recombination rate calculations under different formalisms. *Physical Review B - Condensed Matter and Materials Physics*, 91(20):1–12, 2015.

- [7] Junpei Sukegawa, Christina Schubert, Xiaozhang Zhu, Hayato Tsuji, Dirk M. Guldi, and Eiichi Nakamura. Electron transfer through rigid organic molecular wires enhanced by electronic and electron-vibration coupling. *Nature Chemistry*, 6(10):899–905, 2014.
- [8] Christoph Schnedermann, Antonios M. Alvertis, Torsten Wende, Steven Lukman, Jiaqi Feng, Florian A.Y.N. Schröder, David H.P. Turban, Jishan Wu, Nicholas D.M. Hine, Neil C. Greenham, Alex W. Chin, Akshay Rao, Philipp Kukura, and Andrew J. Musser. A molecular movie of ultrafast singlet fission. *Nature Communications*, 10(1), 2019.
- [9] Timothy J.H. Hele, Bartomeu Monserrat, and Antonios M. Alvertis. Systematic improvement of molecular excited state calculations by inclusion of nuclear quantum motion : A mode-resolved picture and the effect of molecular size. *The Journal of Chemical Physics*, 154:244109, 2021.
- [10] Antonios M. Alvertis, Raj Pandya, Loreta A. Muscarella, Nipun Sawhney, Malgorzata Nguyen, Bruno Ehrler, Akshay Rao, Richard H. Friend, Alex W. Chin, and Bartomeu Monserrat. Impact of exciton delocalization on exciton-vibration interactions in organic semiconductors. *Physical Review B - Condensed Matter and Materials Physics*, 102:081122(R), 2020.
- [11] Florian Brown-Altwater, Gabriel Antonius, Tonatiuh Rangel, Matteo Giantomassi, Claudia Draxl, Xavier Gonze, Steven G. Louie, and Jeffrey B. Neaton. Band gap renormalization, carrier mobilities, and the electron-phonon self-energy in crystalline naphthalene. *Physical Review B*, 101(16):1–12, 2020.
- [12] Venkat Kapil and Edgar A. Engel. A complete description of thermodynamic stabilities of molecular crystals. *Proceedings of the National Academy of Sciences of the United States of America*, 119(6):1–8, 2022.
- [13] Liangyou Fan and Tom Ziegler. Application of density functional theory to infrared absorption intensity calculations on transition-metal Carbonyls. *The Journal of Physical Chemistry*, 96(12):6937–6941, 1992.
- [14] Ming Wah Wong. Vibrational frequency prediction using density functional theory. *Chemical Physics Letters*, 256(4-5):391–399, 1996.
- [15] U. Heinemeyer, R. Scholz, L. Gisslén, M. I. Alonso, J. O. Ossó, M. Garriga, A. Hinderhofer, M. Kytka, S. Kowarik, A. Gerlach, and F. Schreiber. Exciton-phonon coupling in diindenoperylene thin films. *Physical Review B - Condensed Matter and Materials Physics*, 78(8):1–10, 2008.
- [16] Michele Casula, Matteo Calandra, Gianni Profeta, and Francesco Mauri. Intercalant and intermolecular phonon assisted superconductivity in K-doped picene. *Physical Review Letters*, 107(13):1–5, 2011.
- [17] Honghui Shang and Jinlong Yang. Capturing the Electron-Phonon Renormalization in Molecules from First-Principles. *Journal of Physical Chemistry A*, 125(12):2682–2689, 2021.

- [18] Jonathan Laflamme Janssen, Michel Côté, Steven G. Louie, and Marvin L. Cohen. Electron-phonon coupling in C60 using hybrid functionals. *Physical Review B - Condensed Matter and Materials Physics*, 81(7):2–5, 2010.
- [19] R. O. Jones and O. Gunnarsson. The density functional formalism, its applications and prospects. *Reviews of Modern Physics*, 61(3):689–746, 1989.
- [20] J. P. Perdew, K. Burke, and M. Ernzerhof. Generalized Gradient Approximation Made Simple. *Physical Review Letters*, 77:3865, 1996.
- [21] Lars Hedin. New Method for Calculating the One-Particle Green’s Function with Application to the Electron-Gas Problem. *Physical Review*, 139(17):796–823, 1965.
- [22] Mark S. Hybertsen and Steven G. Louie. Electron correlation in semiconductors and insulators: Band gaps and quasiparticle energies. *Physical Review B*, 34(8):5390–5413, 1986.
- [23] Eric L. Shirley and Richard M. Martin. *GW* quasiparticle calculations in atoms. *Phys. Rev. B*, 47:15404–15412, Jun 1993.
- [24] Jeffrey C. Grossman, Michael Rohlfing, Lubos Mitas, Steven G. Louie, and Marvin L. Cohen. High accuracy many-body calculational approaches for excitations in molecules. *Phys. Rev. Lett.*, 86:472–475, Jan 2001.
- [25] C. Rostgaard, K. W. Jacobsen, and K. S. Thygesen. Fully self-consistent *GW* calculations for molecules. *Phys. Rev. B*, 81:085103, Feb 2010.
- [26] X. Blase, C. Attaccalite, and V. Olevano. First-principles *GW* calculations for fullerenes, porphyrins, phthalocyanine, and other molecules of interest for organic photovoltaic applications. *Physical Review B - Condensed Matter and Materials Physics*, 83(11):1–9, 2011.
- [27] Fabien Bruneval. Ionization energy of atoms obtained from *GW* self-energy or from random phase approximation total energies. *J. Chem. Phys.*, 136(19):194107, 2012.
- [28] Xinguo Ren, Patrick Rinke, Volker Blum, Jürgen Wieferink, Alexandre Tkatchenko, Andrea Sanfilippo, Karsten Reuter, and Matthias Scheffler. Resolution-of-identity approach to hartree-fock, hybrid density functionals, rpa, mp2 and *GW* with numeric atom-centered orbital basis functions. *New Journal of Physics*, 14(5):053020, 2012.
- [29] S. Sharifzadeh, I. Tamblyn, P. Doak, P.T. Darancet, and J.B. Neaton. Quantitative molecular orbital energies within a *G0W0* approximation. *Europ. Phys. J. B*, 85(9):323, 2012.
- [30] Thomas Körzdörfer and Noa Marom. Strategy for finding a reliable starting point for *G0W0* demonstrated for molecules. *Phys. Rev. B*, 86:041110, Jul 2012.
- [31] Fabien Bruneval and Miguel A L Marques. Benchmarking the Starting Points of the *GW* Approximation for Molecules. *Journal of Chemical Theory and Computation*, 9(1):324–329, jan 2013.

- [32] M. J. van Setten, F. Weigend, and F. Evers. The gw-method for quantum chemistry applications: Theory and implementation. *J. Chem. Theory Comput.*, 9(1):232–246, 2013. PMID: 26589026.
- [33] P. Koval, D. Foerster, and D. Sánchez-Portal. Fully self-consistent *gw* and quasiparticle self-consistent *gw* for molecules. *Phys. Rev. B*, 89:155417, Apr 2014.
- [34] Marco Govoni and Giulia Galli. Large scale GW calculations. *J. Chem. Theory Comput.*, 11(6):2680–2696, 2015. PMID: 26575564.
- [35] Michiel J. van Setten, Fabio Caruso, Sahar Sharifzadeh, Xinguo Ren, Matthias Scheffler, Fang Liu, Johannes Lischner, Lin Lin, Jack R. Deslippe, Steven G. Louie, Chao Yang, Florian Weigend, Jeffrey B. Neaton, Ferdinand Evers, and Patrick Rinke. GW100: Benchmarking G0W0 for molecular systems. *J. Chem. Theory Comput.*, 11(12):5665–5687, 2015. PMID: 26642984.
- [36] Joseph W. Knight, Xiaopeng Wang, Lukas Gallandi, Olga Dolgounitcheva, Xinguo Ren, J. Vincent Ortiz, Patrick Rinke, Thomas Körzdörfer, and Noa Marom. Accurate ionization potentials and electron affinities of acceptor molecules iii: A benchmark of GW methods. *Journal of Chemical Theory and Computation*, 12(2):615–626, 2016.
- [37] Riichi Kuwahara, Yoshifumi Noguchi, and Kaoru Ohno. GWF + bethe-salpeter equation approach for photoabsorption spectra: Importance of self-consistent GWF calculations in small atomic systems. *Phys. Rev. B*, 94:121116, Sep 2016.
- [38] Xavier Blase, Paul Boulanger, Fabien Bruneval, Marivi Fernandez-Serra, and Ivan Duchemin. *gw* and bethe-salpeter study of small water clusters. *J. Chem. Phys.*, 144(3):034109, 2016.
- [39] Emanuele Maggio, Peitao Liu, Michiel J. van Setten, and Georg Kresse. GW100: A plane wave perspective for small molecules. *Journal of Chemical Theory and Computation*, 13(2):635–648, 2017.
- [40] Malte F. Lange and Timothy C. Berkelbach. On the relation between equation-of-motion coupled-cluster theory and the GW approximation. *J. Chem. Theory Comput.*, 14(8):4224–4236, 2018.
- [41] Dorothea Golze, Jan Wilhelm, Michiel J. van Setten, and Patrick Rinke. Core-level binding energies from gw: An efficient full-frequency approach within a localized basis. *Journal of Chemical Theory and Computation*, 14(9):4856–4869, 2018. PMID: 30092140.
- [42] Jan Wilhelm, Dorothea Golze, Leopold Talirz, Jürg Hutter, and Carlo A. Pignedoli. Toward GW calculations on thousands of atoms. *JPCL*, 9(2):306–312, 2018.
- [43] Alan M. Lewis and Timothy C. Berkelbach. Vertex corrections to the polarizability do not improve the GW approximation for the ionization potential of molecules. *J. Chem. Theory Comput.*, 15(5):2925–2932, 2019. PMID: 30933508.

- [44] Dorothea Golze, Marc Dvorak, and Patrick Rinke. The GW compendium: A practical guide to theoretical photoemission spectroscopy. *Frontiers in Chemistry*, 7:377, 2019.
- [45] Fabien Bruneval, Nike Dattani, and Michiel J. van Setten. The GW Miracle in Many-Body Perturbation Theory for the Ionization Potential of Molecules. *Frontiers in Chemistry*, 9(December):1–12, 2021.
- [46] Carina Faber, Jonathan Laflamme Janssen, Michel Côté, E. Runge, and X. Blase. Electron-phonon coupling in the C60 fullerene within the many-body GW approach. *Physical Review B - Condensed Matter and Materials Physics*, 84(15):30–34, 2011.
- [47] Z. P. Yin, A. Kutepov, and G. Kotliar. Correlation-enhanced electron-phonon coupling: Applications of GW and screened hybrid functional to bismuthates, chloronitrides, and other high-Tc superconductors. *Physical Review X*, 3(2):1–20, 2013.
- [48] G. Antonius, S. Poncé, P. Boulanger, M. Côté, and X. Gonze. Many-body effects on the zero-point renormalization of the band structure. *Physical Review Letters*, 112(21):1–5, 2014.
- [49] Bartomeu Monserrat. Correlation effects on electron-phonon coupling in semiconductors: Many-body theory along thermal lines. *Phys. Rev. B*, 93, 2016.
- [50] Zhenglu Li, Gabriel Antonius, Meng Wu, Felipe H. Da Jornada, and Steven G. Louie. Electron-Phonon Coupling from Ab Initio Linear-Response Theory within the GW Method: Correlation-Enhanced Interactions and Superconductivity in Ba_{1-x}KxBiO₃. *Physical Review Letters*, 122(18):186402, 2019.
- [51] Rodney J. Bartlett and Monika Musiał. Coupled-cluster theory in quantum chemistry. *Reviews of Modern Physics*, 79(1):291–352, 2007.
- [52] Anna Miglio, Véronique Brousseau-Couture, Emile Godbout, Gabriel Antonius, Yang Hao Chan, Steven G. Louie, Michel Côté, Matteo Giantomassi, and Xavier Gonze. Predominance of non-adiabatic effects in zero-point renormalization of the electronic band gap. *npj Computational Materials*, 6(1), 2020.
- [53] Fabio Caruso, Matthias Dauth, Michiel J. Van Setten, and Patrick Rinke. Benchmark of GW Approaches for the GW100 Test Set. *Journal of Chemical Theory and Computation*, 12(10):5076–5087, 2016.
- [54] F. Kaplan, M. E. Harding, C. Seiler, F. Weigend, F. Evers, and M. J. Van Setten. Quasi-Particle Self-Consistent GW for Molecules. *Journal of Chemical Theory and Computation*, 12(6):2528–2541, 2016.
- [55] Marko Schreiber, Mario R. Silva-Junior, Stephan P.A. Sauer, and Walter Thiel. Benchmarks for electronically excited states: CASPT2, CC2, CCSD, and CC3. *Journal of Chemical Physics*, 128(13), 2008.
- [56] Bartomeu Monserrat. Electron – phonon coupling from finite differences. *Journal of Physics Condensed Matter*, 30, 2018.

- [57] Antonios M. Alvertis, Jonah B. Haber, Edgar A. Engel, Sahar Sharifzadeh, and Jeffrey B. Neaton. Phonon-Induced Localization of Excitons in Molecular Crystals from First Principles. *Physical Review Letters*, 130(8):86401, 2023.
- [58] Christopher E. Patrick and Feliciano Giustino. Unified theory of electron–phonon renormalization and phonon-assisted optical absorption. *Journal of Physics: Condensed Matter*, 26:365503, 2014.
- [59] G. Kresse, J. Furthmüller, and J. Hafner. Ab initio Force Constant Approach to Phonon Dispersion Relations of Diamond and Graphite. *Europhysics Letters*, 32:729, 1995.
- [60] K. Parlinski, Z. Q. Li, and Y. Kawazoe. First-Principles Determination of the Soft Mode in Cubic ZrO₂. *Physical Review Letters*, 78:4063, 1997.
- [61] Axel D. Becke. A new mixing of Hartree-Fock and local density-functional theories. *The Journal of Chemical Physics*, 98(2):1372–1377, 1993.
- [62] E. Aprà *et al.* NWChem: Past, present, and future. *The Journal of chemical physics*, 152(18):184102, 2020.
- [63] Rachel Crespo-Otero and Mario Barbatti. Spectrum simulation and decomposition with nuclear ensemble: Formal derivation and application to benzene, furan and 2-phenylfuran. *Theoretical Chemistry Accounts*, 131(6):1–14, 2012.
- [64] Bartomeu Monserrat, Edgar A. Engel, and Richard J. Needs. Giant electron-phonon interactions in molecular crystals and the importance of nonquadratic coupling. *Phys. Rev. B*, 92(14):1–6, 2015.
- [65] Axel D. Becke. A new mixing of Hartree–Fock and local density-functional theories. *The Journal of Chemical Physics*, 98(2):1372–1377, 01 1993.
- [66] D. M. Ceperley and B. J. Alder. Ground state of the electron gas by a stochastic method. *Physical Review Letters*, 45(7):566–569, 1980.
- [67] Fabien Bruneval, Ivan Maliyov, Clovis Lapointe, and Mihai-Cosmin Marinica. Extrapolating Unconverged GW Energies up to the Complete Basis Set Limit with Linear Regression. *Journal of Chemical Theory and Computation*, 16(7):4399–4407, jul 2020.
- [68] Cannada A. Lewis, Justus A. Calvin, and Edward F. Valeev. Clustered Low-Rank Tensor Format: Introduction and Application to Fast Construction of Hartree-Fock Exchange. *Journal of Chemical Theory and Computation*, 12(12):5868–5880, 2016.
- [69] Chong Peng, Justus A. Calvin, Fabijan Pavošević, Jinmei Zhang, and Edward F. Valeev. Massively Parallel Implementation of Explicitly Correlated Coupled-Cluster Singles and Doubles Using TiledArray Framework. *Journal of Physical Chemistry A*, 120(51):10231–10244, 2016.

- [70] Diptarka Hait and Martin Head-Gordon. Delocalization Errors in Density Functional Theory Are Essentially Quadratic in Fractional Occupation Number. *Journal of Physical Chemistry Letters*, 9(21):6280–6288, 2018.

Supplementary Information to ‘Capturing electronic correlations in electron-phonon interactions in molecular systems with the *GW* approximation’

Antonios M. Alvertis^{1,2,*}, David B. Williams-Young³, Fabien Bruneval⁴, Jeffrey B. Neaton^{2,5,6,†}

¹KBR, Inc., NASA Ames Research Center, Moffett Field, California 94035, United States

²Materials Sciences Division, Lawrence Berkeley National Laboratory, Berkeley, California 94720, United States

³Applied Mathematics and Computational Research Division, Lawrence Berkeley National Laboratory, Berkeley, California 94720,
United States

⁴Université Paris-Saclay, CEA, Service de Corrosion et de Comportement des Matériaux, SRMP, 91191 Gif-sur-Yvette, France

⁵Department of Physics, University of California Berkeley, Berkeley, United States

⁶Kavli Energy NanoScience Institute at Berkeley, Berkeley, United States

*e-mail: amalvertis@lbl.gov

†e-mail: jbneaton@lbl.gov

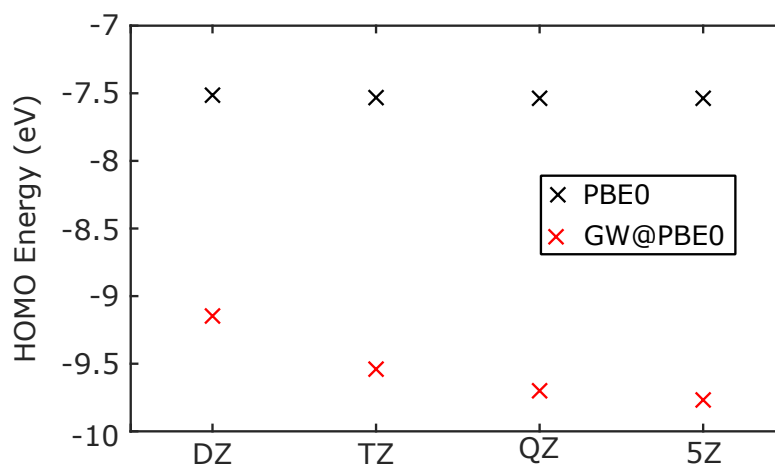


Figure 1 Convergence of the HOMO energy of pyrimidine within DFT-PBE0 and $GW@PBE0$, with respect to the size of the basis set aug-cc-pVX, with X assuming the values of the x-axis.

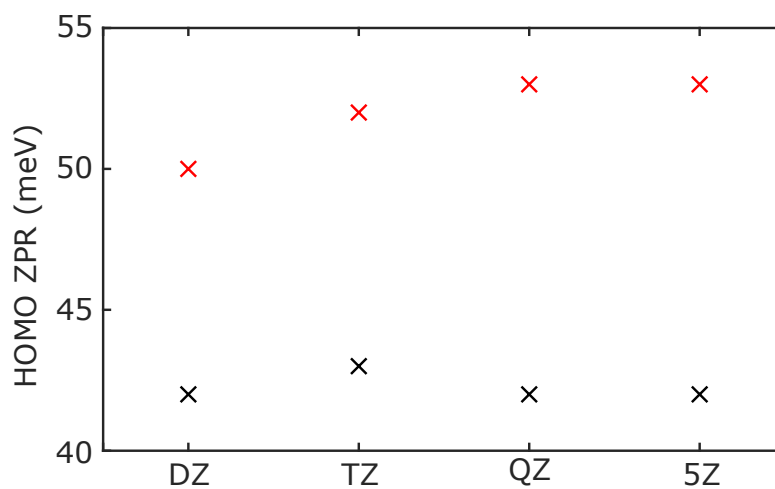


Figure 2 Convergence of the HOMO ZPR of pyrimidine within DFT-PBE0 and $GW@PBE0$, with respect to the size of the basis set aug-cc-pVX, with X assuming the values of the x-axis.

system	PBE	PBE0	PBEh	BHLYP
acetamide	-0.014	0.016	0.036	0.035
acetone	-0.014	0.008	0.031	0.026
adenine	0.002	-0.004	-0.007	-0.01
benzene	-0.004	-0.009	-0.014	-0.018
benzoquinone	0.038	0.045	0.143	0.204
butadiene	0.009	-0.005	-0.002	-0.005
cyclopentadiene	-0.015	-0.014	-0.012	-0.016
cyclopropene	0.104	0.111	0.115	0.105
cytosine	0.082	0.017	0.014	0.012
ethene	0.011	0.006	0.002	-0.003
formaldehyde	0.029	0.048	0.067	0.067
formamide	-0.054	0	0.059	0.064
furan	0.014	0.015	0.016	0.015
hexatriene	-0.016	-0.011	-0.006	-0.011
imidazole	0.014	0.01	0.008	0.005
naphthalene	-0.013	-0.009	-0.006	-0.014
norbornadiene	-0.004	0.001	0.007	0.003
octatetraene	-0.027	-0.025	-0.021	-0.027
propanamide	-0.051	-0.016	0.026	0.028
pyrazine	0.024	0.064	0.064	0.009
pyridazine	-0.001	0.023	0.056	0.058
pyridine	0.022	0.062	0.063	0.056
pyrimidine	0.022	0.043	0.073	0.068
pyrrole	-0.001	0.001	0.004	0.001
tetrazine	0.006	0.026	0.041	0.043
thymine	0.018	0.017	0.016	0.015
triazine	0.019	0.039	0.065	0.067
uracil	0.047	0.014	0.007	0.006

Table 1 Zero-point renormalization of the energy of the highest occupied molecular orbital of the Thiel set molecules within density functional theory and employing the different functionals given here. All values are in eV.

system	GW@PBE	GW@PBE0	GW@PBEh	GW@BHLYP	IP-EOM-CCSD
acetamide	0.066	0.063	0.044	0.038	0.044
acetone	0.069	0.058	0.053	0.049	0.05
adenine	-0.003	0.005	0.001	0.0013	0.004
benzene	0	-0.006	-0.01	-0.01	-0.008
benzoquinone	0.087	0.069	0.057	0.053	0.092
butadiene	0.008	0.007	0.004	0.005	0.002
cyclopentadiene	0.007	0.002	-0.001	-0.002	-0.002
cyclopropene	0.146	0.137	0.131	0.128	0.146
cytosine	0.025	0.034	0.032	0.033	0.031
ethene	0.011	0.008	0.005	0.006	0.012
formaldehyde	0.057	0.058	0.059	0.058	0.059
formamide	0.022	0.048	0.069	0.066	0.072
furan	0.033	0.028	0.026	0.028	0.031
hexatriene	0.004	0.001	-0.001	-0.002	-0.005
imidazole	0.028	0.025	0.02	0.022	0.029
naphthalene	0.002	0	-0.002	-0.007	-0.002
norbornadiene	0.028	0.022	0.018	0.018	0.017
octatetraene	-0.01	-0.016	-0.018	-0.021	-0.025*
propanamide	0.022	0.024	0.021	0.016	0.036
pyrazine	0.067	0.085	0.011	0.107	0.091
pyridazine	0.04	0.037	0.04	0.033	0.038
pyridine	0.071	0.09	0.087	0.088	0.07
pyrimidine	0.055	0.052	0.034	-0.004	0.055
pyrrole	0.019	0.015	0.013	0.014	0.02
tetrazine	0.041	0.041	0.041	0.04	0.037
thymine	0.024	0.031	0.026	0.03	0.029
triazine	0.053	0.047	0.051	0.047	0.05
uracil	0.108	0.032	0.025	0.027	0.027

Table 2 Zero-point renormalization of the energy of the highest occupied molecular orbital of the Thiel set molecules within coupled cluster (IP-EOM-CCSD) and the *GW* approximation using a starting point of density functional theory with the different functionals given here. All values are in eV. *The IP-EOM-CCSD values for octatetraene have been obtained within the smaller aug-cc-pVDZ basis set, due to memory issues encountered when employing aug-cc-pVTZ.